An Evaluation of the Annular Fuel and Bottle-Shaped Fuel Concepts for Sodium Fast Reactors

An Evaluation of the Annular Fuel and Bottle-shaped Fuel Concepts for Sodium Fast Reactors

Matthew Memmott, Jacopo Buongiorno*, Pavel Hejzlar
Nuclear Science and Engineering Department
Massachusetts Institute of Technology (MIT)
77 Massachusetts Ave., 02139 Cambridge MA, * jacopo@mit.edu, +1(617)253-7316

Abstract

Two innovative fuel concepts, the internally and externally cooled annular fuel and the bottle-shaped fuel, were investigated with the goal of increasing the power density and reduce the pressure drop in the sodium-cooled fast reactor, respectively. The concepts were explored for both high- and low-conversion core configurations, and metal and oxide fuels. The annular fuel concept is best suited for low-conversion metal-fuelled cores, where it can enable a power uprate of ~20%; the magnitude of the uprate is limited by the fuel clad chemical interaction temperature constraint during a hypothetical flow blockage of the inner-annular channel. The bottle-shaped fuel concept is best suited for tight high-conversion ratio cores, where it can reduce the overall core pressure drop in the fuel channels by >30%, with a corresponding increase in core height between 15 and 18%. A full-plant RELAP5-3D model was created to evaluate the transient performance of the innovative fuel configurations during the station blackout and unprotected transient over power. The transient analysis confirmed the good thermal-hydraulic performance of the annular and bottle-shaped fuel designs with respect to the reference case with traditional solid fuel pins.

Keywords: power density, pressure drop, sodium coolant
Number of Pages: 38
Number of Tables: 7
Number of Figures: 12

1. Introduction

The economic performance of sodium-cooled fast reactors (SFR), like that of any nuclear system, benefits from high power density and low pressure drop (pumping power) in the core. The purpose of this paper is to describe a study of two innovative fuel configurations that aim at increasing the SFR core power density and reducing its pumping power, while maintaining the safety margins and the neutronic performance of the traditional SFR core designs. The innovative fuel configurations explored here are the internally/externally cooled annular fuel and the bottle-shaped fuel concepts.

Annular UO_2 fuel with internal and external cooling has been studied at MIT for over 6 years, for both BWRs [1] and PWRs [2] where it can enable power density increases of up to 50%. The large heat transfer surface attainable with simultaneous internal and external cooling reduces the fuel operating temperature and the surface heat flux dramatically. The feasibility of annular fuel oxide pellets was also demonstrated at the Columbia Westinghouse fuel fabrication plant in Columbia, SC, in the context of the same MIT-led project [2]. Annular fuel can potentially enhance the thermal (and economic) performance of SFRs as well.

In SFRs the fuel rod plenum accounts for up to ~40% of the overall fuel rod length, yet does not produce any power and is not subject to major neutronic restrictions. Bottle-shaped fuel refers to a fuel rod whose diameter is smaller in the plenum region than in the active core region, which results in a significant decrease in the overall core pressure drop. To maintain a constant gas plenum volume, the length of the gas plenum region must be increased.

The innovative fuel configurations are described in Section 3 of this paper. Their thermal performance at steady-state conditions is evaluated in Section 4, while the performance during transients is discussed in Section 5.

2. Reference Core and Fuel Designs

The annular and bottle-shaped fuel configurations will be compared to the more traditional designs outlined by Hoffman et al. [3], which include both high and low conversion ratio (CR) designs, with metal and oxide fuels. Table I and Figure 1 show the core and fuel configurations of the breakeven (CR=1.0) and burner (CR=0.25) designs developed by Hoffman et al. In addition to these high and low bounding conversion ratios, an intermediate conversion ratio core of CR = 0.71, is listed in Table I. This conversion ratio is included because it is the selected conversion ratio for the ABR1000 concept.

3. Conceptual Design of Innovative Fuel Configurations

3.1 Annular Fuel

Annular fuel for the sodium fast reactor is designed by increasing the overall fuel rod diameter and introducing an inner flow channel in the center of the fuel rod, which is separated from the fuel by an additional clad and bond layer. A cross-section depiction of the annular fuel rod design compared to the traditional solid fuel pin design is seen in Fig. 2. As the rod outer diameter is significantly larger, the number of fuel rods per assembly must be decreased, in order to maintain a nearly constant assembly size, as shown in Fig. 3.

A parametric study of various geometries was conducted to identify the most promising configuration for the annular fuel assemblies (FA). In the analysis, the following parameters were held equal to the corresponding reference designs:

- The fuel-to-coolant volume ratio and the core height, which preserves the overall neutronic characteristics of the core (i.e., spectrum, reactivity coefficients, reactivity letdown) to first order. Note, however, that annular fuel has a little bit more cladding material, thus a small neutronic penalty is expected.
- Fuel smeared density, which allows for adequate accommodation of fuel swelling under irradiation.
- Inter-assembly gap and FA duct thickness, which provide adequate FA clearance and mechanical robustness, respectively.
- Core power density, which ensures the fairness of the initial comparison between solid and annular FAs. Obviously our objective is to increase the power density, as will be explained later.

The gap between the FA duct and the adjacent fuel pins was set at a reasonable value of 0.3 mm to enable sliding of the fuel pin bundle into the duct during fabrication and to allow for swelling and thermal expansion. The wire helical pitch was held at 20.32 cm. Also, the inner diameter of the annular fuel pins is limited to ≥3.5 mm, as smaller channels are deemed susceptible to clogging.

In comparing the annular FA designs to the reference designs, two figures of merit were adopted: the average heat flux at the clad surface, q'', and the radial temperature rise in the fuel, ΔT (i.e., the difference between the maximum temperature in the fuel, T_{max}, and the temperature on the fuel surface, T_{fo}). Everything else being the same (i.e., sodium inlet temperature and flow rate, power density), it is clear that FA designs with lower q'' and ΔT

will also have lower clad and fuel temperatures, thus allowing for potential power uprates. Using the above constraints and figures of merit, the parametric study demonstrated that the annular fuel approach is most promising for the low-conversion cores, as their high P/D_o value allows for easy accommodation of the annular fuel pins. On the other hand, use of annular fuel pins in the high-conversion cores would be problematic due to the tightness of the fuel pin array, which does not allow for a good balance of flow between the inner and outer channels. Therefore, here only the results for the burner core configurations are discussed. Table II reports the optimal geometry of the annular fuel assemblies developed for the oxide and metal fuel burner cores. The details of the parametric study leading to this optimal geometry are in Ref. 4.

3.2 Bottle-shaped Fuel

The core flow area and the hydraulic diameter both contribute inversely to the pressure drop in the core. Therefore, by decreasing the radius of the fuel rod in the plenum region (and simultaneously increasing its length, thus maintaining the necessary plenum volume for fission gas collection), the pressure drop in the plenum region can be significantly decreased. The fuel rod pitch remains constant in the fuel plenum region, so the gap between fuel rods is larger there, which calls for the use of grid spacers (vs wire wrap) in the plenum region. A representation of the bottle-shaped fuel is shown in Fig. 4.

A parametric study of various geometries was again conducted to identify the most promising configuration for the bottle-shaped FA. In the analysis the following parameters were held equal to the corresponding reference core designs:

- The active core region geometric parameters including core height, rod lattice pitch, rod diameters, core mass flow rate, and wire-wrap dimensions.

- Core thermal and neutronic properties, such as power profiles, power generation rate, and neutronic performance, e.g., neutron spectrum, reactivity coefficients, reactivity letdown.
- Fuel assembly pitch in both core and gas plenum regions
- Shielding thickness and assembly entrance/exit configurations.

In order to ensure the stability of the fuel rods in the plenum region, it was assumed that a grid spacer was needed for every 0.5 meters of plenum length, and that the grid spacers were triagonal honey-combed spacers with a thickness of 0.5 mm.

In comparing the bottle-shaped FA designs to the reference designs, two figures of merit were adopted: the total pressure drop across the core, and the total fuel rod length or core height. Everything else being the same (i.e., sodium inlet temperature and flow rate, pitch), FAs with lower pressure drop across the plenum will also have a lower pressure drop across the entire core, thus allowing for lower pumping costs. The parametric study (all details reported in Ref. 4) indicated that the bottle-shaped fuel is most beneficial to high conversion ratio cores since relaxation of the tighter pitch results in greater pressure drop reductions. Therefore, here only the parameters for the breakeven core configurations and the CR = 0.71 core configurations are reported, as seen in Table III. However, since the breakeven design is a bounding case, while the CR = 0.71 core is more likely configuration for the ABR1000 [5], the rest of the bottle-shaped fuel analyses were focused only on the CR = 0.71 core.

4. Subchannel Analysis

To better quantify the performance of the new annular fuel and bottle-shaped FA, a subchannel analysis was conducted using a RELAP5-3D model created specifically for the analysis of non-traditional fuel configurations. The use and validation of RELAP5-3D as a subchannel tool is discussed in a separate paper [6] and will not be repeated here. The goal of the subchannel analysis was to determine the magnitude of the power uprates for the annular fuel designs, and the reduction in pressure drop across the core for the bottle-shaped fuel designs. For all fuel configurations, the friction factor and heat transfer correlations described in Cheng and Todreas [7] were used for the triangular, edge and corner subchannels. In the annular FA, the friction factor in the inner channels was evaluated using the Blasius correlation for smooth round tubes [8]. In the bottle-shaped FA the form pressure drop associated with the flow expansion at the inlet of the plenum region was modeled with the correlation [9]:

$$K = \left(1 - \frac{1}{n}\right)^2, \qquad n = \frac{A_{fp}}{A_{fc}} \tag{1}$$

where:

A_{fp} = flow area in the plenum subchannels (post-expansion)

A_{fc} = flow area in the core subchannels (pre-expansion).

Moreover, previous studies [6] have indicated that the inclusion of vertical duct "ribs" in the edge subchannels, as shown in Fig. 5, allows for a much flatter temperature distribution across the FA; therefore, the reference, annular and bottle-shaped fuel configurations were

all modeled using these duct ribs. The radial (hot fuel assembly) power peaking factor used for all fuel configurations was assumed to be 1.2. The axial power peaking was 1.16 and 1.23 for the oxide and metal fuel designs, respectively. Local inter-assembly peaking in fast reactors is very small (2-4%) and was therefore neglected in this study. The thermal conductivity for the burner core fuel (both metal and oxide) were taken from Hoffman et al. [3] , while the conductivity for the breakeven core fuel were taken from Ref. 10(metal) and the RELAP5 internal material property tables (oxide). In all cases the thermal conductivity of the cladding was taken from the RELAP5 property tables. The RELAP5 model for gap conductance was used for the oxide fuel gap, while simple conduction through the sodium bond was assumed for the metal fuel gap.

4.1 Reference Fuel

The steady-state coolant temperature distribution for the reference FA is shown in Fig. 6. Due to the inclusion of ribs, the coolant temperature distribution is rather flat. Note that the reference burner core FAs include also "structural" steel rods (depicted in red), as per the original design by Hoffman et al. [3] . These un-fuelled rods are incorporated throughout the assembly to support the weight of the grid spacers, since the fuel rods have such a small outer diameter in the burner core [3] . Structural rods are not required in annular fueled FAs as the fuel rods are quite large and self supported by wire wrap.

4.2 Annular Fuel

The steady-state coolant temperature distribution for the annular fuel assemblies is shown in Fig. 7, while the core pressure drop, and maximum fuel and clad temperatures are

reported in Table IV. Note that Fig. 7 and the "nominal annular" column in Table IV are for the same power density as the reference core. The annular fuel concept realizes a dramatic reduction in fuel temperatures and also a substantial reduction in clad temperatures, albeit at the expense of a higher pressure drop. To quantify the magnitude of the power uprate afforded by the annular fuel concept, we increased the linear power (and proportionally the coolant flow rate, to maintain the same outlet temperature) until the pressure drop in the core doubled with respect to the nominal case. The corresponding power uprates are 40% for the oxide fuel and 45% for the metal fuel, as shown in Table IV ("uprated annular" column). Note that even at these higher power densities, the fuel and clad temperatures in the annular FA are lower than the fuel and clad temperatures in the reference FA. In other words, the pressure drop increase is more restrictive than the limits on fuel and clad temperatures, at least at steady-state.

With annular fuel, the potential for flow blockage in the inner channels must be evaluated. We postulated complete blockage of the flow through the hottest inner channel in the fuel assembly. The subchannel analysis for this case shows that the coolant temperature in the blocked channel would be well over 1000°C for the oxide fuel, but only 674°C for the metal fuel. In the oxide fuel case, sodium would completely boil off in the blocked channel leading to clad rupture. Therefore, it was concluded that the annular fuel concept is not feasible for oxide fuels. The more benign behavior of the metal fuel is obviously due to its much higher thermal conductivity, so that if the inner channel is blocked, all the heat produced in the rod is conducted out to the coolant surrounding the rod. Since a single-channel blockage event may be difficult to detect, it was assumed that flow blockage

should be subject to the steady-state limits. The postulated steady-state limit for the clad in metal fuel is 650°C, which should prevent excessive fuel clad chemical interaction and clad creep [11,12]. At 674°C the clad temperature in the blocked channel is still too high. As such, the magnitude of the uprate in the annular metal FA was reduced until the clad temperature in the blocked channel decreased to 650°C, which corresponded to a power uprate of 20% (see Table IV). This number is approximate since the analysis included the peaking factors, but not all the engineering uncertainties. Significant thermal stresses develop in the clad due to differential expansion during the blockage accident. These stresses are tensile in the outer clad and compressive in the inner clad. While the stresses are well below the yield strength of steel at 650°C, they would be sufficient to cause buckling of the inner clad, if the clad were unsupported. In reality, the clad is supported by the fuel matrix itself all along the active section of the rod. Nevertheless, this is clearly an area warranting more attention in the future. The details of the structural analysis are in Ref. 4.

4.3 Bottle-Shaped Fuel

The coolant temperature distribution for the bottle-shaped FA could not be distinguished from that of the reference fuel, which was expected because the bottle-shaped fuel does not alter the core geometry in the active region. However, the total core pressure drop was greatly reduced, 31 and 36% in the oxide and metal core, respectively, at the expense of a modest increase in overall core length (see Table V). The stresses in the truncated cone connecting the clad in the active region to the clad in the gas plenum region were analyzed and found to be well within the ASME code limits [4]. Some open questions remain for the

bottle-shaped fuel concept, e.g., the fabrication feasibility and costs, the availability of space above the core to accommodate the longer fuel rods, the impact on the reactivity coefficients (it was assumed in this study that the reactivity coefficients remained the same between the two configurations, though in reality they may be different, in particular the radial expansion and the coolant void coefficients.)

5. Safety Analysis

The innovative fuel designs were evaluated with respect to their ability to safely survive the SFR design-basis accidents, i.e., the unprotected transient overpower (UTOP) and the station blackout, the latter effectively subsuming the unprotected loss of flow and loss of heat sink events. The most restrictive safety limit is the clad temperature, which must be kept below the value at which excessive clad creep and fuel clad chemical interaction occur. For metal fuels this limit can be assumed to be around 750°C [11]. For oxide fuels the temperature limit is approximately the same, though it is limited by the potential for mechanical failure rather than Pellet-Cladding Chemical Interaction (PCCI) [12]. A RELAP5-3D model of the SFR plant was created (Figs 8 and 9). The model comprises the core, the reactor pool (primary sodium), the intermediate heat transfer system (IHTS, or secondary sodium), the power conversion system (PCS) and the direct reactor auxiliary cooling system (DRACS). The core model comprises six parallel channels representing the lumped inner driver assemblies, the outer driver assemblies, the hottest assembly, the control assemblies, the shield assemblies, and the reflector assemblies. The four IHTS loops and their related PCSs were also lumped to reduce model runtime. Note that the PCS is modeled as a simple boundary condition (inlet feedwater temperature and flow rate) for

the steam generator, which is a suitable approach for simulating the UTOP and station blackout events.

An unprotected station blackout accident is defined by the loss of all electrical power to the plant, the failure of emergency backup power and failure to scram. Under these conditions, the heat sink (PCS) is lost, the pumps stop working, and DRACS initiates. For the station blackout transients analyzed here, the PCS is assumed to be lost instantly upon accident initiation, while the pumps continue to operate at progressively decreasing speeds for a period of time. This gradual decrease in pump speed after accident initiation is called the pump "coast-down." A coastdown halving time of 20 seconds is utilized in this study. Additionally, only 2-out-of-3 DRACS trains are assumed to operate normally, while it is assumed that the 3rd fails to initiate.

The UTOP accident is defined by the insertion of reactivity due to the removal of a control rod with the highest worth. This results in an upward ramp of the core power until the negative feedbacks push the core power back down. The core power reaches an equilibrium value that is slightly higher than the original steady-state core power. Two types of UTOP were considered: a slow rod withdrawal (0.9¢/s for the metal cores and 0.53¢/s for the oxide cores, up to a final reactivity insertion of $0.70) and a rod ejection accident (stepwise insertion of $0.70 reactivity). The rod ejection accident is very unlikely, perhaps impossible, in a system operating at low pressure; however it was included as a bounding event.

Six core models were created to represent six fuel configurations: the metal CR = 0.71 reference fuel, the oxide CR = 0.71 reference fuel, the metal CR = 0.71 bottle-shaped fuel, the oxide CR = 0.71 bottle-shaped fuel, the metal CR = 0.25 base fuel, and the metal CR = 0.25 annular fuel. The annular oxide case was not considered because its steady-state performance is not acceptable, as explained in Section 4 above.

In the annular CR = 0.25 core, the assemblies were larger, and thus a new core layout (Fig 10) was developed in which the power generation was only 950 MW. This means that a 20 % power uprate results in a power of 1140 MW, or 11.4% over the reference core configuration. The PCS and DRACS capacities were increased accordingly.

A point kinetics approach with the reactivity feedbacks used in the ABR1000 [5], as shown in Table VI, was used for the various core configurations. The details of the RELAP5 models, including dimensions and operating conditions for all components are reported in Ref. 4.

A summary of the cases analyzed and their respective results are found in Table VII.

The fuel and clad temperature history for the CR=0.25 cores (both reference and uprated annular) during the station blackout and UTOP are shown in Figs 11 and 12, respectively. Note that the uprated annular fuel core performs similarly or better than the reference solid fuel core in both transients. The clad limits are satisfied with margin in both transients. A detailed description of the transients follows.

It can be seen in Fig. 11 that both the solid and uprated annular fuel configurations have similar trends: initially the clad and coolant temperatures increase because the pumps tripped, while the fuel temperature decreases because the power is reduced by the reactivity feedback. The peak at around 100 s is due to the power dropping below the heat removal capacity ensured by the pump coast down.

The trends for both the metal CR = 0.25 uprated annular and solid fuels are very similar, with slight differences in magnitude and peak location. It is significant to note that the fuel temperature in the annular design is very close to the clad temperature, and significantly lower than the fuel temperature for the reference solid pin design at the beginning of the transient. After the peak, all temperatures are fairly close with differences within the model uncertainties.

In the station blackout, there is also a second long-term temperature peak (not shown in Fig. 11) due to the DRACS heat removal capacity finally exceeding the core decay power. Prior to this point, the DRACS heat removal system removes slightly less heat than the core decay power produces, resulting in a gradual temperature rise. As the core decay power drops below the DRACS heat removal capabilities, the temperature peaks, and then begins to decrease again. This second peak is significantly lower than the first peak, and does not challenge the FCCI limits.

In the UTOP accident (shown in Fig. 12), both solid and uprated annular CR = 0.25 fuel configurations experience an increase in power, thus the temperature increases rapidly. As

the temperature increases, the reactivity feedbacks reduce the power, and a new equilibrium is reached at a power and temperature that are higher than the original steady state values.

Note that the annular fuel temperature is significantly lower than the solid fuel temperature, while its clad temperature is slightly higher.

Finally, the bottle-shaped fuel cores (figures not shown here) were found to perform identically to the reference fuel in the UTOP, and slightly better than the reference fuel in the station blackout, due to its lower pressure drop, which enhances natural circulation during events in which the pumps are lost.

Conclusions

The concepts of annular and bottle-shaped fuel were explored for use in the sodium-cooled fast reactor, as they offer potential for higher power density and lower pressure drop in the core, respectively. The thermal-hydraulic performance of these innovative fuel configurations was evaluated by means of steady-state subchannel analyses and transient plant analyses, both conducted with the RELAP5-3D code. The main findings from these analyses were as follows:

- The annular fuel concept enables an increase of the power density by 20% in low-conversion-ratio (burner) cores with metal fuels. It was also shown that annular metal fuel can survive a complete flow blockage of the hottest inner channel.
- The annular fuel concept is not suitable for oxide fuel cores because flow blockage of the hottest inner channel would lead to sodium boiling and excessive clad temperatures.

- The bottle-shaped fuel affords a reduction of the core pressure drop by over 30% in the higher-conversion-ratio (CR = 0.71) cores with both metal and oxide fuels.
- Both fuel concepts yield similar or better fuel and clad temperatures than the reference cores during the unprotected transient overpower and station blackout events.

Acknowledgements

The U.S. Department of Energy and the U.S. Nuclear Regulatory Commission are gratefully acknowledged for their Nuclear Engineering and Health Physics (NE/HP) Fellowship and the Nuclear Education Fellowship, respectively, awarded to Matthew Memmott during his studies at MIT. Special thanks to Cliff Davis of the Idaho National Laboratory (INL), for extensive guidance and assistance in creating and utilizing the RELAP5-3D models. Also, thanks is given to Matt Denman for investigating the neutronic aspects of the annular fuel configurations.

References

1. M. S. Kazimi, J. Buongiorno, T. Conboy, T. Ellis, P. Ferroni, P. Hejzlar, S-P. Kao, A. Karahan, K. Kobayashi, E. Pilat, N.E. Todreas, “Core Design Options for High Power Density BWRs”, MIT Report NFC-PR-089, December 2006.
2. P. Hejzlar P. and M.S. Kazimi, “Annular Fuel for High Power Density PWRs: Motivation and Overview“, Nuclear Technology, 160, 2-15, (2007).

3. E. Hoffman et al., “Preliminary Core Design Studies for the Advanced Burner Reactor over a Wide Range of Conversion Ratios”, ANL Report ANL-AFCI-177, September, 2006.

4. Memmott M., J. Buongiorno, P. Hejzlar, 2009, Thermal-Hydraulic Analysis of Innovative Fuel Configurations for the Sodium Fast Reactor, Report MIT-ANP-TR-123, Center for Advanced Nuclear Energy Systems (CANES), Massachusetts Institute of Technology, Cambridge MA.

5. Y.I. Chang, P.J.Finck, C. Grandy, et al., “Advanced Burner Test Reactor Preconceptual Design Report”, ANL-ABR-1 (ANL-AFCI-173), September, 2006

6. M. J. Memmott, J. Buongiorno, P. Hejzlar, "On the Use of RELAP5-3D as a Subchannel Analysis Code", Nuclear Engineering and Design, 240, 807–815, 2010, 2009.

7. S. K. Cheng and N. E. Todreas, “Hydrodynamic Models and Correlations for Bare and Wire-Wrapped Hexagonal Rod Bundles – Bundle Friction Factors, Subchannel Friction factors and Mixing Parameters” Nuclear Engineering and Design, 92, 227-251, (1986).

8. N. E. Todreas, M. S. Kazimi, *Nuclear Systems I. Thermal Hydraulic Fundamentals*, pg. 379, Taylor and Francis, 1993

9. I. E. Idelchik, “Handbook of Hydraulic Resistance Second Edition”, pg. 233-235, Hemisphere Publishing Corporation, New York, USA, 1986.

10. M. C. Billone et al., "Status of Fuel Element Modeling Codes for Metallic Fuels", Proceedings American Nuclear Society International Conference on Reliable Fuels for Liquid Metal Rectors, Tuscon Arizona, September 7-11, 1986.

11. A. B. Cohen, H. Tsai, and L. A. Neimark, “Fuel/cladding compatibility in U-19Pu-10Zr/HT9-clad fuel at elevated temperatures”, Journal of Nuclear Materials, Vol. 204, pg 244-251, 1993.

12. R. B. Baker et al., “Performance of Fast Flux Test Facility Driver and Prototype Driver Fuels”, WHC-SA-0974, (1990).

Table I: Core configuration of breakeven, burner and most probable cores [3,5]

	CR = 0.25		CR = 1.0		CR = 0.71	
	Metal	**Oxide**	**Metal**	**Oxide**	**Metal**	**Oxide**
Driver assemblies	151	151	144	144	180	180
-Inner	19	19	48	72	78	78
-Middle	66	66	54	36	0	0
-Outer	66	66	42	36	102	102
Blanket	0	0	0	0	0	0
Primary control assemblies	9	9	22	16	15	15
Secondary control assemblies	3	3	3	3	4	4
Gas expansion modules	0	0	0	0	0	0
Reflector assemblies	90	138	84	102	114	114
Shield assemblies	60	60	60	60	66	66
Fuel pins per assembly	540	324	271	271	271	271
Bond material	Na	He	Na	He	Na	He
Height (core), cm	101.6	137.16	101.6	137.16	81.29	106.68
Height (plenum), cm	191.14	170.82	191.14	170.82	124.40	160.02
Overall pin length	407.04	422.28	407.04	422.28	477.52	477.52
Fuel smeared density, %TD	75	85	75	85	75	85
Fabrication density, %TD	100	89.4	100	89.4	100	89.4
Pin diameter, cm	0.464	0.556	0.808	0.868	0.755	0.755
Pin pitch-to-diameter ratio	1.357	1.448	1.163	1.023	1.18	1.18
Cladding thickness, cm	0.0559	0.0635	0.0559	0.0635	0.056	0.056
Inter-assembly gap, cm	0.432	0.432	0.432	0.432	0.432	0.432
Assembly duct thickness, cm	0.394	0.394	0.394	0.394	0.394	0.394
Wire-wrap diameter, cm	*	*	0.0805	0.0195	0.131	0.131
Core Power, MW	1000	1000	1000	1000	1000	1000
Power Density, kW/L	258	191	258	191	303	231
Mass Flow Rate, kg/s	5024	5024	5024	5024	5024	5024
Inlet Temperature, °C	355	355	355	355	355	355
Outlet Temperature, °C	510	510	510	510	510	510
Volume fraction, %						
-fuel	31.02	49.29	17.44	19.73	29.2	37.0
-bond	10.34	2.55	5.81	1.02	9.8	2.0
-structure	24.16	28.58	29.15	26.22	25.7	25.7
-coolant	34.48	19.58	47.60	53.02	35.3	35.3

*Reference burner core design has loose lattice with spacers

Table II: Design parameters of burner core reference and annular FAs for both metal and oxide fuels

	Metal, CR = 0.25		Oxide, CR = 0.25	
	Reference	**Annular**	**Reference**	**Annular**
Rings	13	11	10	9
Pins	540	397	324	271
Flat to flat (cm)	15.71	18.29	15.71	15.74
Pin outer diameter (mm)	4.64	7.67	5.56	7.85
Pin inner diameter (mm)	-	3.6	-	3.6
P/Do	1.357	1.11	1.45	1.14
Dwire (mm)	*	1.0	*	1.1
Clad thickness (mm)	0.559	0.559	0.635	0.635
Fuel volume fraction (%)	17.48	16.03	19.73	17.48
Bond volume fraction (%)	5.83	5.33	1.02	0.22
Structure volume fraction (%)	28.55	34.98	26.22	37.71
Coolant volume fraction (%)	48.13	43.68	53.02	43.91
Fuel/coolant volume ratio	0.366	0.366	0.372	0.398
Wire-wrap helical pitch (cm)	-	20.32	-	20.32

* Reference burner core design has loose lattice with spacers

Table III: Design parameters of breakeven and ABR1000 cores of the reference and bottle-shaped FAs for both metal and oxide fuels

	CR = 1.0 (base)		CR = 1.0 (bottle)		CR = 0.71 (base)		CR = 0.71 (bottle)	
	Metal	**Oxide**	**Metal**	**Oxide**	**Metal**	**Oxide**	**Metal**	**Oxide**
Height (core), cm	101.6	137.16	101.6	137.16	81.29	106.68	81.30	106.69
Height (plenum), cm	191.14	170.82	254.7	248.3	124.40	160.02	144.72	186.15
Overall pin length	407.04	422.28	470.54	499.56	477.52	477.52	497.84	503.65
Fuel smeared density, %TD	75	85	75	85	75	85	75	85
Fabrication density, %TD	100	89.4	100	89.4	100	89.4	100	89.4
Pin diameter (core), cm	0.808	0.868	0.808	0.868	0.755	0.755	0.755	0.755
Pin Diameter (plenum), m	0.808	0.868	0.700	0.720	0.755	0.755	0.700	0.700
Pin pitch-to-diameter ratio (core)	1.163	1.023	1.163	1.023	1.18	1.18	1.18	1.18
Pin pitch-to-diameter ratio (plenum)	1.163	1.023	1.342	1.233	1.18	1.18	1.27	1.27
Cladding thickness, cm	0.0559	0.0635	0.0559	0.0635	0.056	0.056	0.056	0.056
Inter-assembly gap, cm	0.432	0.432	0.432	0.432	0.432	0.432	0.432	0.432
Assembly duct thickness, cm	0.394	0.394	0.394	0.394	0.394	0.394	0.394	0.394
Wire-wrap diameter, cm	0.0805	0.0195	0.0805	0.0195	0.131	0.131	0.131	0.131
Power Density, kW/L	268	198	268	198	303	231	303	231

Table IV: Results of subchannel analyses for reference, nominal annular, and uprated annular fuel designs (oxide and metal)

	Oxide			Metal			
	Reference	**Nominal Annular**	**Uprated Annular**	**Reference**	**Nominal Annular**	**Uprated Annular**	**Uprated Annular (blockage limited)**
Core ΔP (MPa)	0.078	0.2735	0.547	0.108	0.209	0.414	0.303
Max Clad Temperature (°C)	579.63	560.28	564.67	578.73	560.96	568.04	639.97*
Max Fuel Temperature (°C)	1821.25	688.22	750.95	694.36	458.6	592.89	639.97*
Power Uprate (%)	-	-	40	-	-	45	20
Average Coolant Velocities (m/s)							
Inner	-	5.17	7.72	-	5.35	7.83	6.45
Triangular	3.93	4.54	6.7	4.31	4.52	6.52	5.41
Edge	2.98	4.75	5.26	3.27	3.44	4.95	4.11
Corner	3.07	3.6	5.31	3.67	3.49	5.02	4.17

* The maximum fuel and inner clad temperatures are the same when the inner channel is fully blocked.

Table V: Core pressure drop for bottle-shaped and reference FA (CR = 0.71)

	Metal	Oxide
Optimal plenum radius (mm)	3.5	3.5
Plenum height (m)	1.45	1.86
Bottle-shaped to reference core height ratio	1.04	1.05
Pressure drop in reference assembly (kPa)	458.6	458.6
Pressure drop in bottle-shaped assembly (kPa)	257.15	293.27
Reduction (%)	43.9	36.1

Table VI: BOEC core reactivity feedback coefficients for each core model (These are typical values for the SFR, and are based upon the ABR1000 core[5])

	Metal CR = 0.71 core	Oxide CR = 0.71 core	Metal CR = 0.25 reference core	Metal CR = 0.25 annular core
Effective delayed neutron fraction	0.00335	0.00316	0.0027	0.0027
Prompt neutron lifetime (μs)	0.36	0.48	0.44	0.44
Radial expansion coefficient (¢/°C)	-0.39	-0.32	-0.48	-0.48
Axial expansion coefficient (¢/°C)	-0.05	-0.05	-0.63	-0.63
Fuel density coefficient (¢/°C)	-0.71	-0.46	-0.93	-0.93
Vessel expansion coefficient (¢/°C)	0.06	0.07	0.1	0.1
Sodium temperature coefficient (¢/°C)	0.11	0.1	0.18	0.18
Doppler coefficient (¢/°C)	-0.13	-0.16	-0.06	-0.12

Table VII: Transient analyses performed with summary of results

* = reference - = worse than ref + = better than ref	X = meets limits X = meets limits w/ changes X = does not meet limits		UTOP		Station blackout
			Slow rod withdrawal	Rod ejection	
Metal	Base	CR = 0.25	*	*	*
		CR = 0.71	*	*	*
	Bottle-shaped	CR = 0.25			
		CR = 0.71			+
	Annular	CR = 0.25	-/+	-/+	-/+
		CR = 0.71			
Oxide	Base	CR = 0.25			
		CR = 0.71	*	*	*
	Bottle-shaped	CR = 0.25			
		CR = 0.71			+
	Annular	CR = 0.25			
		CR = 0.71			

FIGURE CAPTIONS

Figure 1: (a) Breakeven (CR=1) core design for both oxide and metal fuels. (b) Burner (CR=0.25) core designs for oxide (left) and metal (right) fuel. (Figures taken from [3])

Figure 2: Annular fuel rod (left) vs traditional solid fuel rod (right). (drawing to scale)

Figure 3: Annular fuel rod assembly (right) vs traditional solid fuel rod assembly (left). (drawing to scale)

Figure 4: Segments of the reference (left) and bottle-shaped fuel pins (right) (drawing to scale)

Figure 5: Cross-sectional view of a rib (green semi-circle) along the duct wall

Figure 6: Core outlet temperatures (in °C) for reference core designs. (a) burner – oxide, (b) burner – metal, (c) CR = 0.71– oxide, (d) CR = 0.71 – metal.

Figure 7: Core outlet temperatures for annular FA: (a) oxide and (b) metal. (The #s within each circle represent the outlet coolant temperature of the corresponding annular fuel rod inner channels)

Figure 8: Nodalization diagram of the RELAP5-3D model for the reactor pool.

Figure 9: Nodalization diagram of the RELAP5 model for (a) the intermediate loop and steam generator, (b) DRACS.

Figure 10: Core layout for annular fuel metal CR = 0.25 core

Figure 11: Maximum clad and fuel temperatures for the metal CR = 0.25 fuel configurations during a station blackout event with 20 second pump coast-down

Figure 12: Maximum clad and fuel temperatures for the metal CR = 0.25 fuel configurations during a UTOP accident.

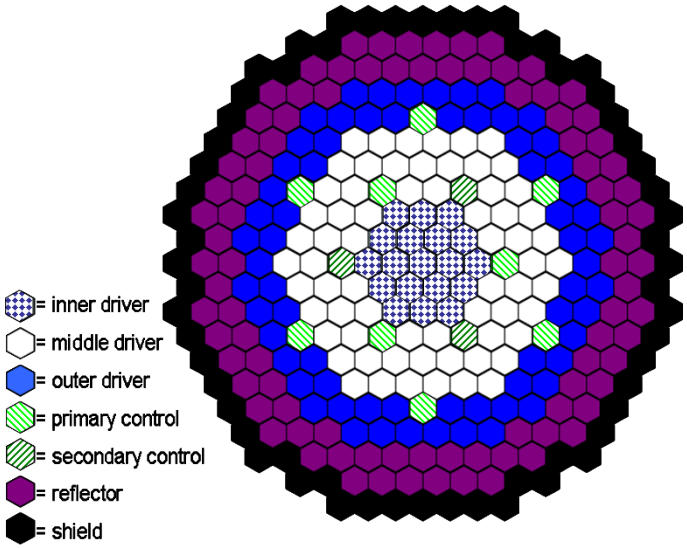

(a)

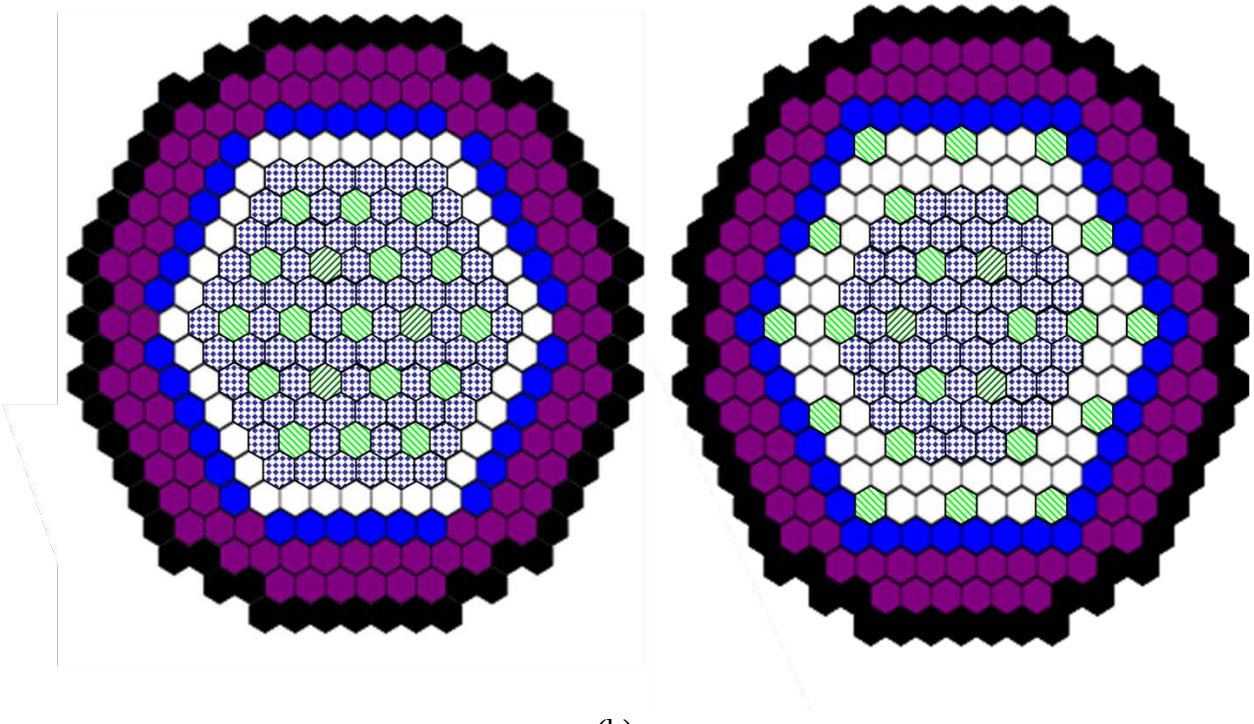

(b)

Figure 1: (a) Breakeven (CR=1) core design for both oxide and metal fuels. (b) Burner (CR=0.25) core designs for oxide (left) and metal (right) fuel.
(Figures taken from [3])

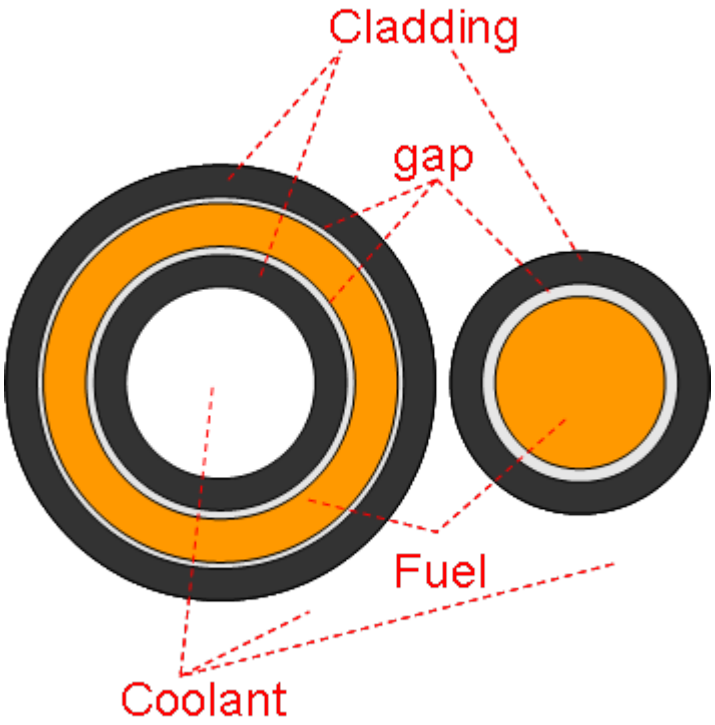

Figure 2: Annular fuel rod (left) vs traditional solid fuel rod (right). (drawing to scale)

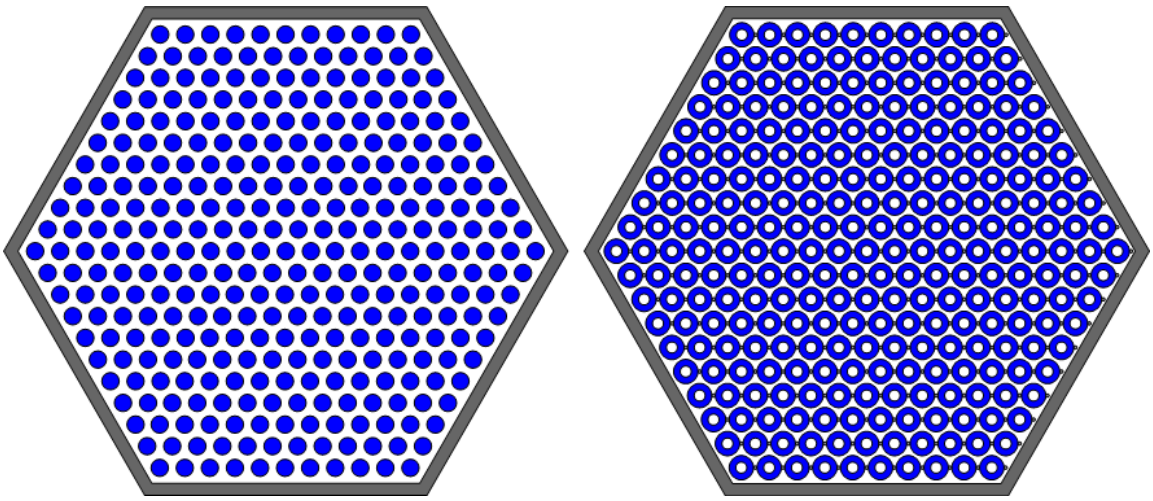

Figure 3: Annular fuel rod assembly (right) vs traditional solid fuel rod assembly (left). (drawing to scale)

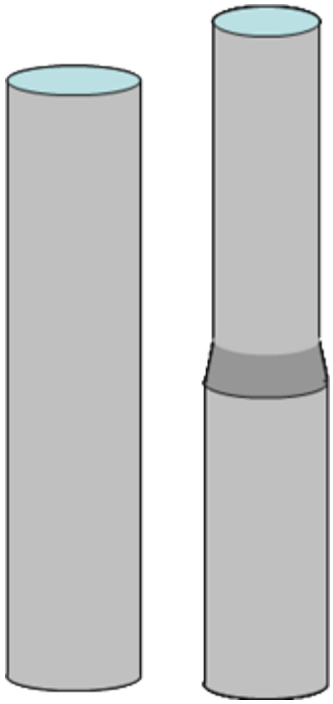

Figure 4: Segments of the reference (left) and bottle-shaped fuel pins (right) (drawing to scale)

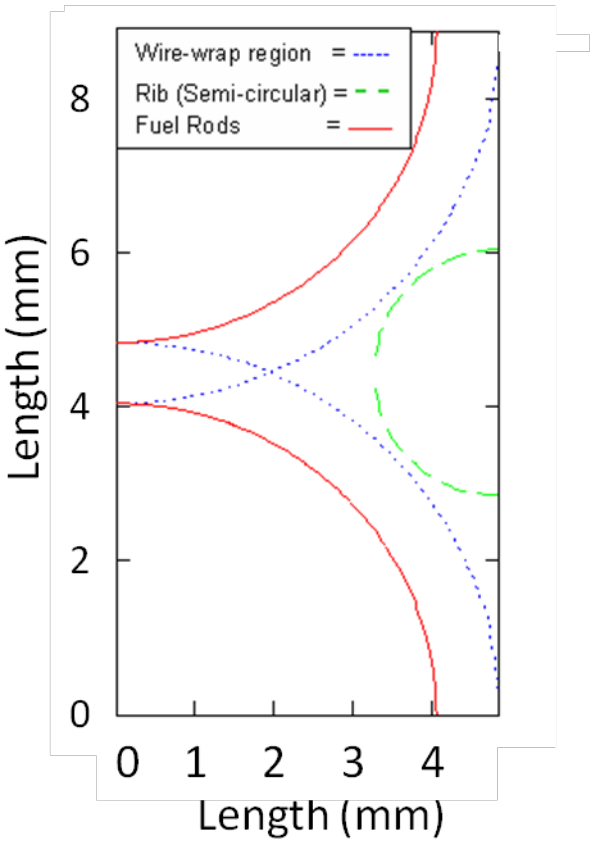

Figure 5: Cross-sectional view of a rib (green semi-circle) along the duct wall

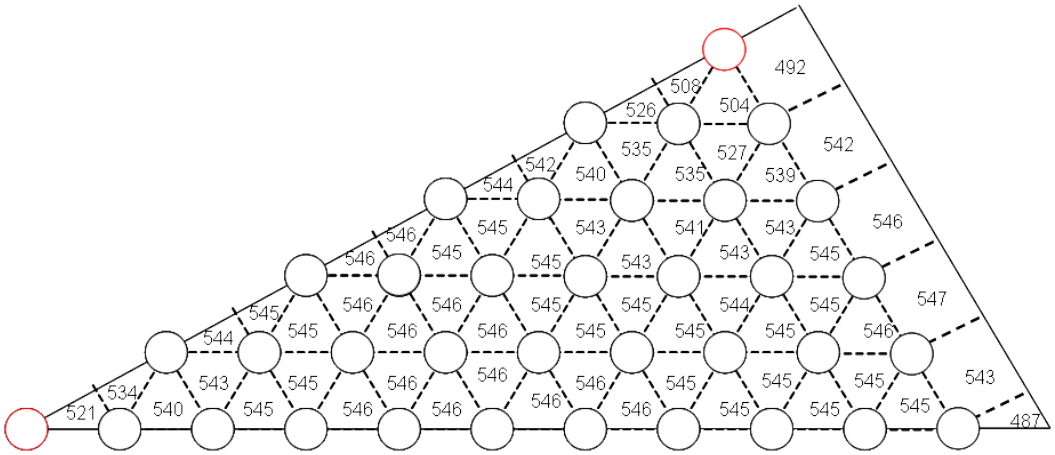
492
508
526
504
535
527
542
542
540
535
539
544
546
545
543
541
543
546
546
545
545
543
543
545
545
546
547
545
546
546
545
545
544
545
546
544
545
546
546
546
545
545
545
543
534
543
545
546
546
546
546
545
545
545
545
543
521
540
545
546
546
546
545
545
487

(a)

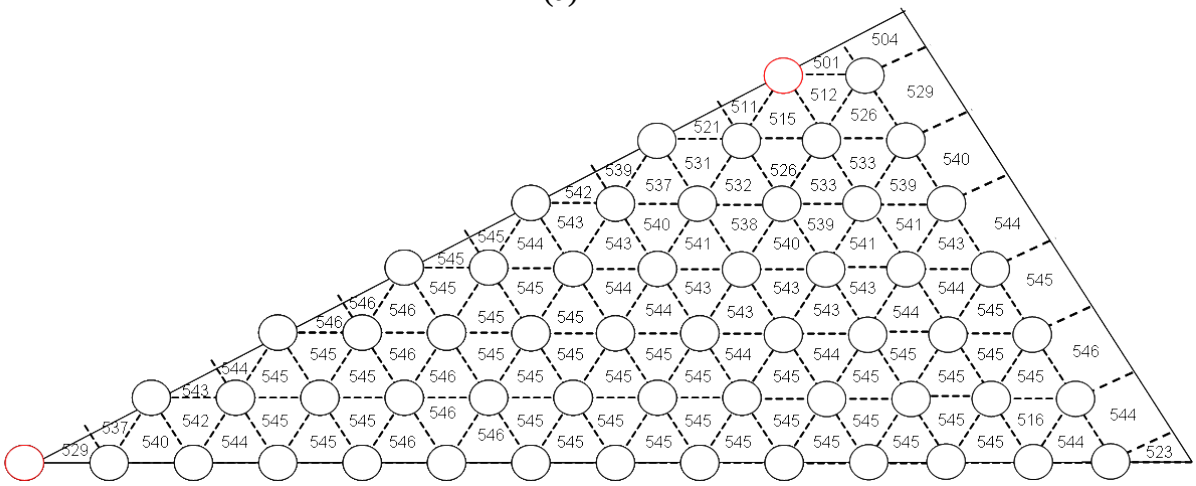
504
501
529
512
526
511
515
521
540
531
526
533
539
537
532
542
544
543
540
538
539
541
543
545
544
543
541
540
541
545
545
544
543
543
543
544
544
545
546
546
545
545
544
544
545
545
546
544
545
545
545
545
545
545
545
545
545
545
545
543
542
545
545
546
546
545
545
545
545
545
545
545
516
544
537
540
544
545
545
546
546
545
545
545
545
545
545
545
545
544
529
523

(b)

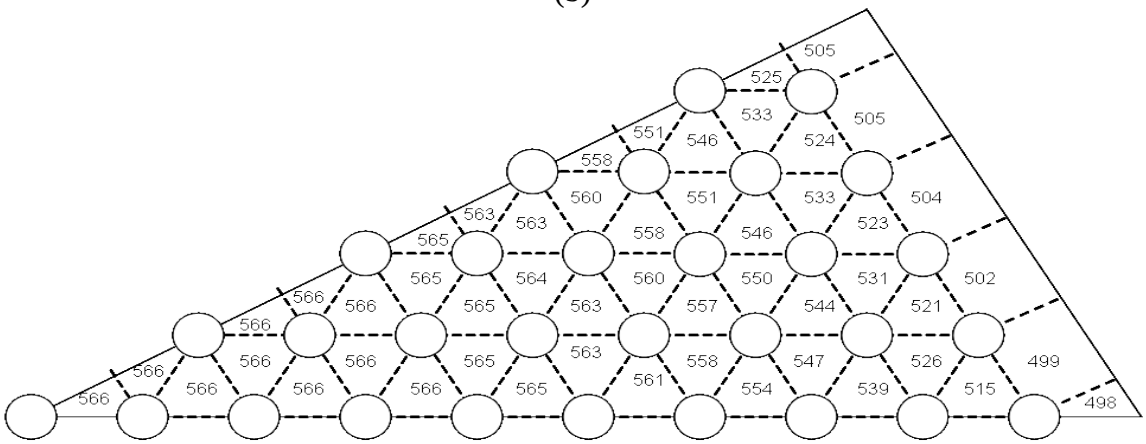
505
525
533
505
551
546
524
558
560
551
533
504
563
563
558
546
523
565
565
564
560
550
531
502
566
566
565
563
557
544
521
566
566
566
565
563
558
547
526
499
566
566
566
566
565
561
554
539
515
498

(c)

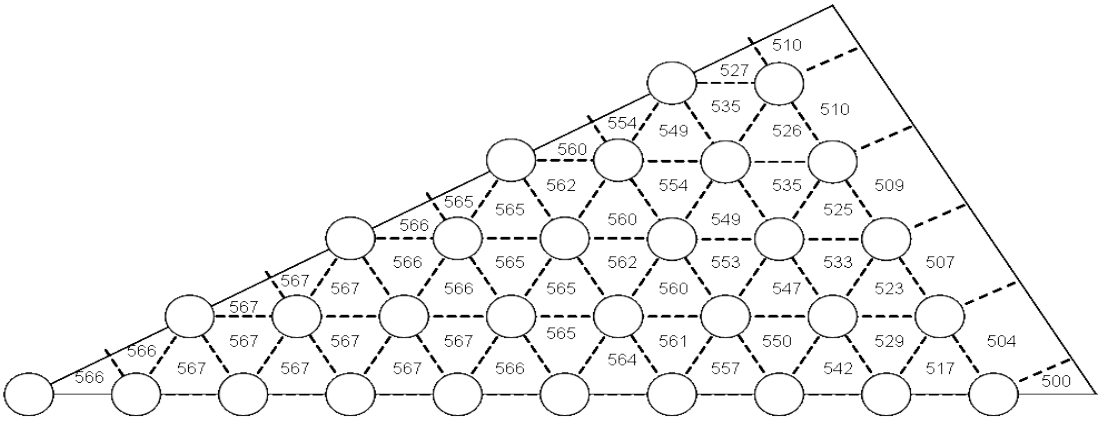

(d)

Figure 6: Core outlet temperatures (in °C) for reference core designs. (a) burner – oxide, (b) burner – metal, (c) CR = 0.71– oxide, (d) CR = 0.71 – metal.

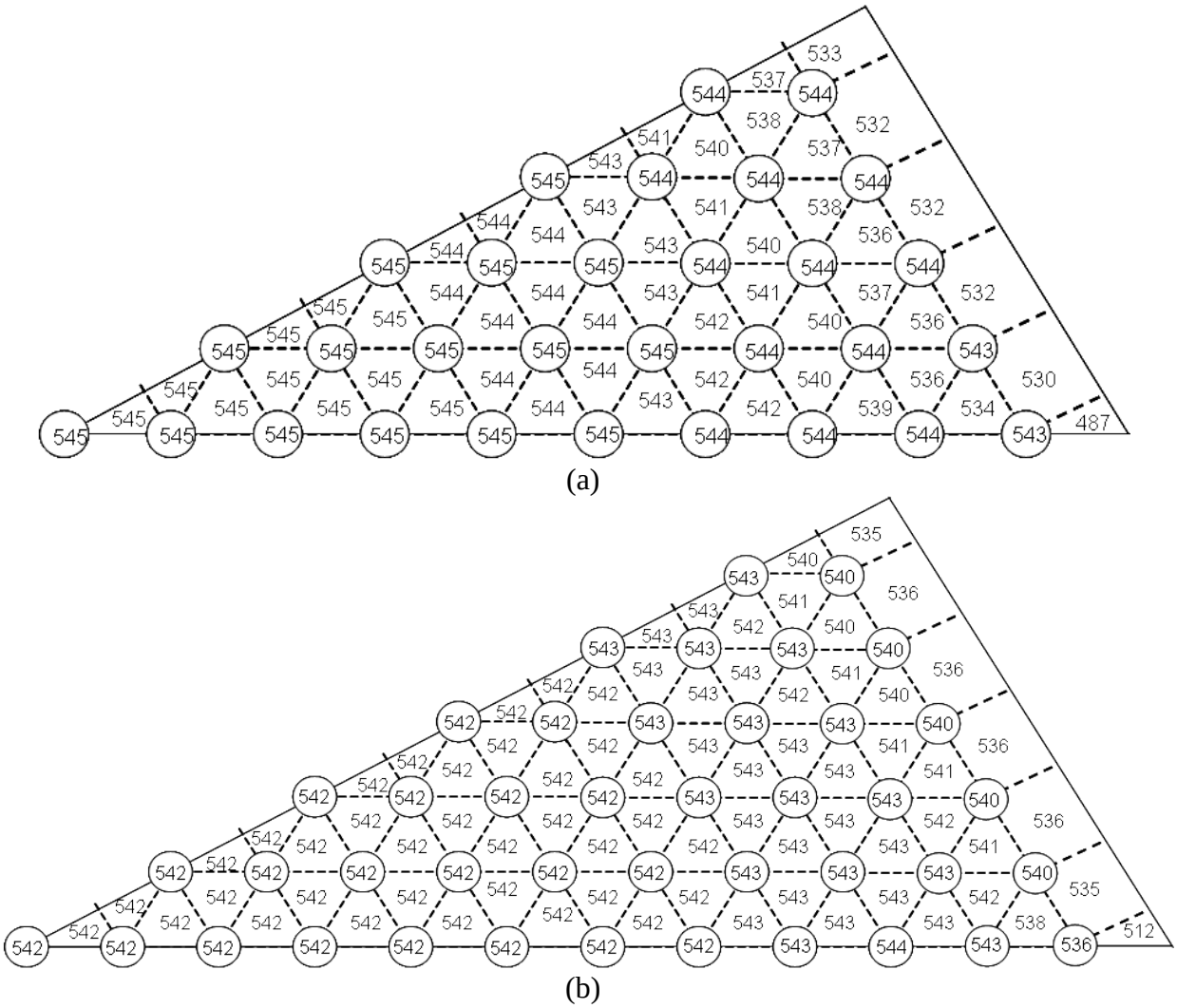

Figure 7: Core outlet temperatures for annular FA: (a) oxide and (b) metal. (The #s within each circle represent the outlet coolant temperature of the corresponding annular fuel rod inner channels)

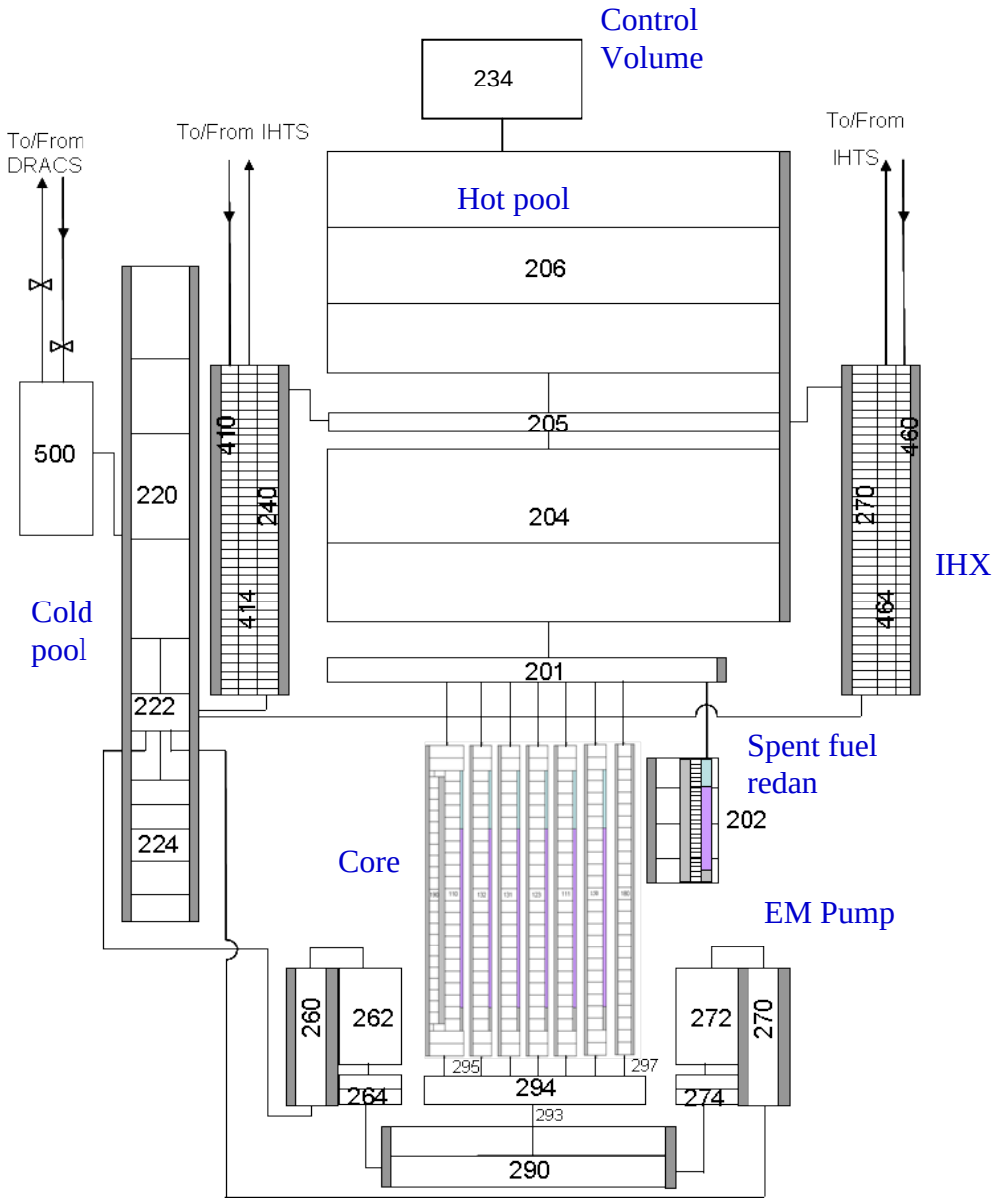

Figure 8: Nodalization diagram of the RELAP5-3D model for the reactor pool.

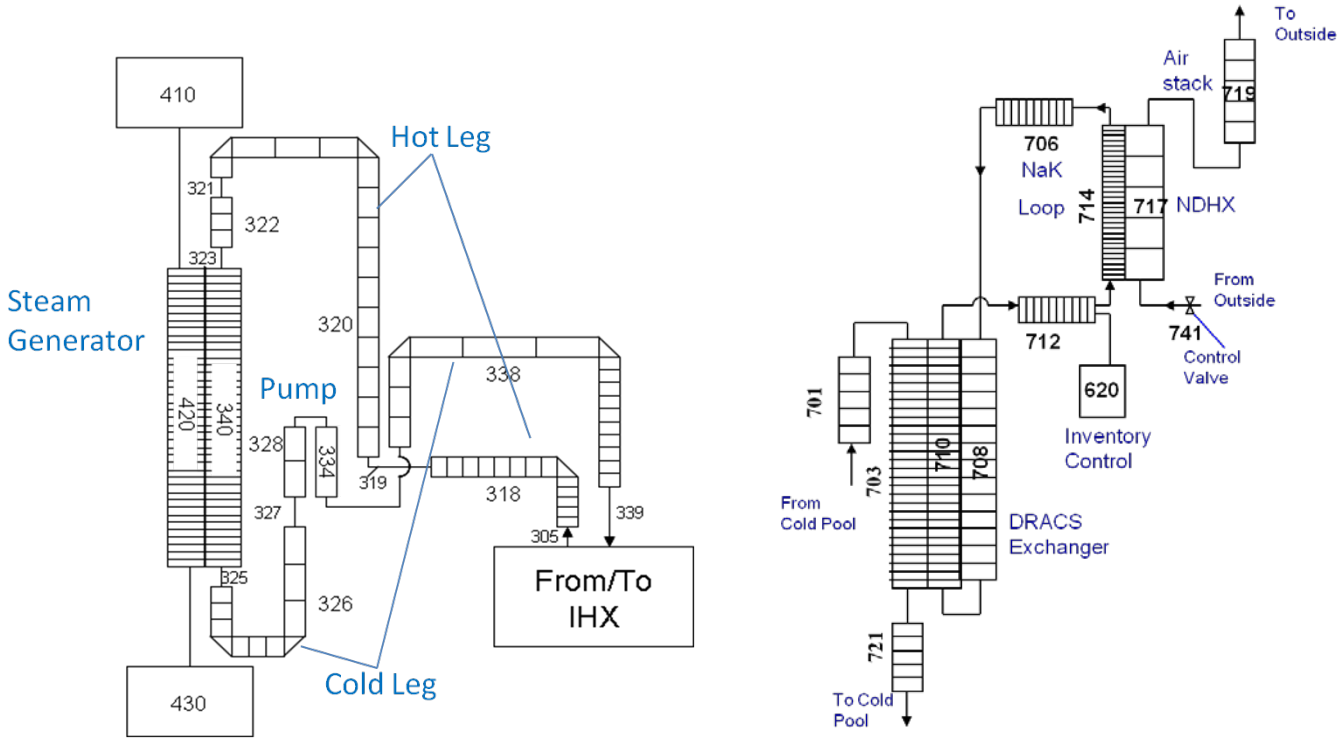

Figure 9: Nodalization diagram of the RELAP5 model for (a) the intermediate loop and steam generator, (b) DRACS.

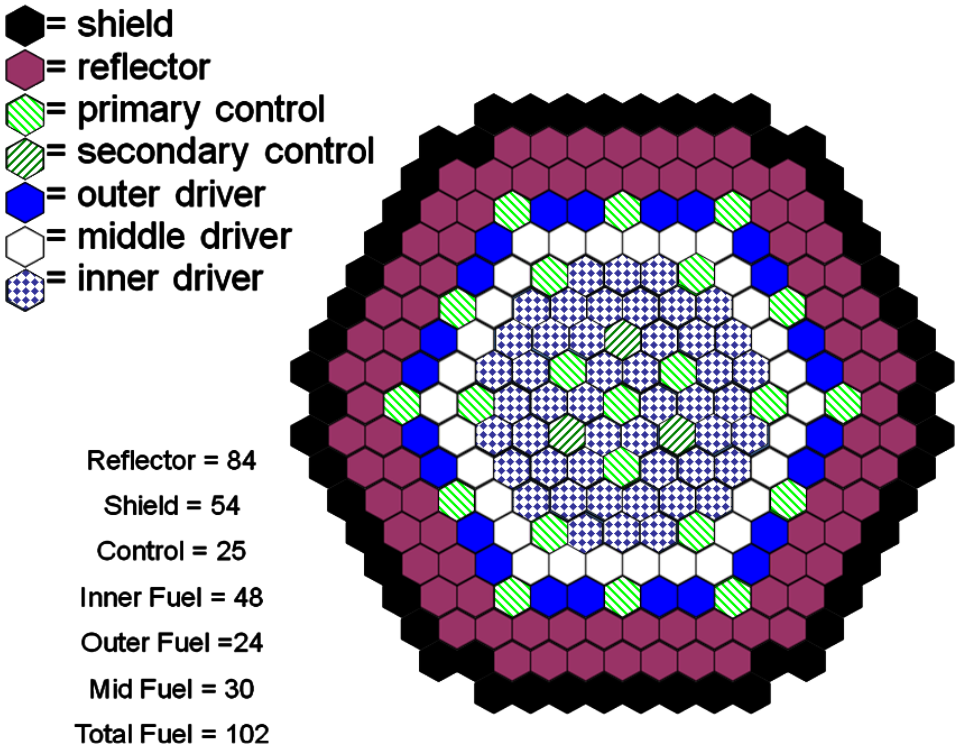

Figure 10: Core layout for annular fuel metal CR = 0.25 core

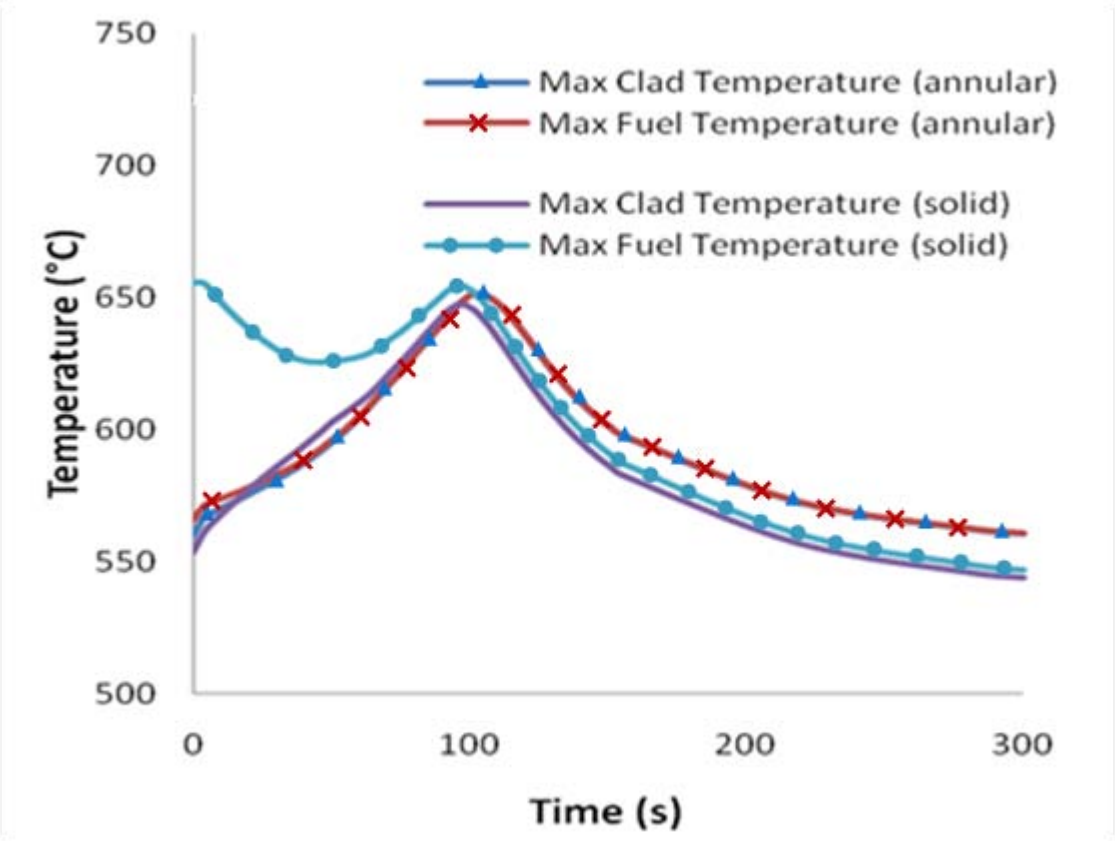

Figure 11: Maximum clad and fuel temperatures for the metal CR = 0.25 fuel configurations during a station blackout event with 20 second pump coast-down

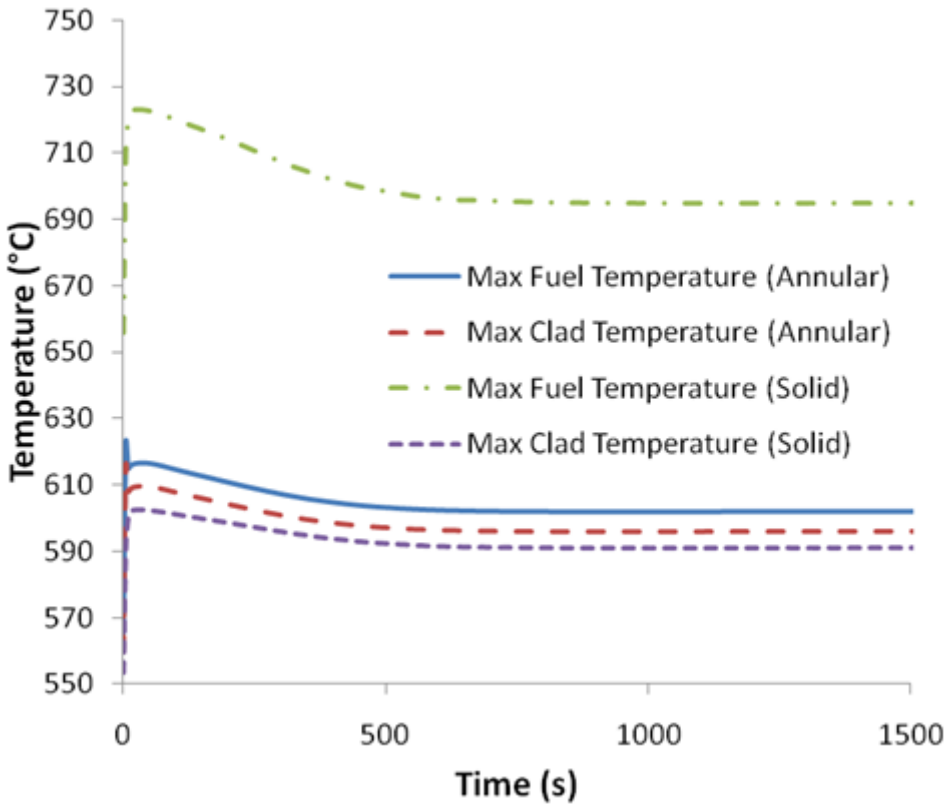

Figure 12: Maximum clad and fuel temperatures for the metal CR = 0.25 fuel configurations during a UTOP accident